Influence of secondary treatment with CO_2 laser irradiation for mitigation site on fused silica surface*

Yong Jiang(蒋勇)[1,3], Qiang Zhou(周强)[1], Rong Qiu(邱荣)[1], Xiang Gao(高翔)[1], Hui-Li Wang(王慧丽)[1], Cai-Zhen Yao(姚彩珍)[2], Jun-Bo Wang(王俊波)[1], Xin Zhao(赵鑫)[1], Chun-Ming Liu(刘春明)[3], Xia Xiang(向霞)[3], Xiao-Tao Zu(祖小涛)[3], Xiao-Dong Yuan(袁晓东)[2], and Xin-Xiang Miao(苗心向)[2,†]

[1] *Joint Laboratory for Extreme Conditions Matter Properties, Southwest University of Science and Technology, Mianyang* 621010, *China*
[2] *Research Center of Laser Fusion, China Academy of Engineering Physics, Mianyang* 621900, *China*
[3] *School of Physical Electronics, University of Electronic Science and Technology of China, Chengdu* 610054, *China*

(Received 29 January 2016; revised manuscript received 22 June 2016; published online 25 August 2016)

The ablation debris and raised rim, as well as residual stress and deep crater will be formed during the mitigation of damage site with a CO_2 laser irradiation on fused silica surface, which greatly affects the laser damage resistance of optics. In this study, the experimental study combined with numerical simulation is utilized to investigate the effect of the secondary treatment on a mitigated site by CO_2 laser irradiation. The results indicate that the ablation debris and the raised rim can be completely eliminated and the depth of crater can be reduced. Notable results show that the residual stress of the mitigation site after treatment will reduce two-thirds of the original stress. Finally, the elimination and the controlling mechanism of secondary treatment on the debris and raised rim, as well as the reasons for changing the profile and stress are analyzed. The results can provide a reference for the optimization treatment of mitigation sites by CO_2 laser secondary treatment.

Keywords: fused silica, CO_2 laser, numerical simulation, secondary treatment

PACS: 81.40.Wx, 42.70.Ce, 78.20.Bh, 61.80.Ba **DOI:** 10.1088/1674-1056/25/10/108104

1. Introduction

Fused silica is one of the most important optical components in fusion class laser systems, such as the National Ignition Facility (NIF) in USA, the Laser Mega Joule in France and the SG-III laser facility in China.[1] With the improvement of facility fluence, the various defects (such as scratches, indentations) and contaminations on optics will lead to the various negative effects on the system. For example, the formation of a strong light field resulting from the light modulation of defects,[2] the appearance of localized high temperature because of laser energy absorbed by impurities,[3] etc., each will lead to an easier damage event of optics. Moreover, the catastrophic damage will occur if the initiation damage grows under the subsequent laser shots, leading to the great loss of performance of optics, such as transmission, damage resistance ability. Many methods, including etching the damage by hydrofluoric acid (HF) in the ultrasound environment,[4] and localized CO_2 laser irradiation,[5–7] have been put forward to suppress the damage growth. Presently, the CO_2 laser treatment is recognized as one of the most effective and promising methods.

Two methods, i.e., evaporative and non-evaporative mitigation technique,[8] are used to mitigate the damage growth of the damage site. The non-evaporative approach is a more suitable technique for the damage site where the depth is less than 100 μm, while the evaporative approach should be chosen for deeper damage sites. However, the disadvantage of the evaporative method is more obvious than that of the non-evaporative one. For example, a larger residual stress will be produced by the evaporative method than that by the non-evaporative method under irradiation of the same-size laser beam. Furthermore, the deposited ablation debris and raised rim formed in the evaporative mitigation process are easier to produce around the mitigated site.[8] It is shown that residual stress will lead to the crack propagation once the re-initiation damage of the mitigation site takes place.[9] The ablation debris will reduce the damage resistance of optics,[10] and the raised rim will modulate the transmitted light, even leading to the damage of downstream optics.[11]

To avoid those negative effects, one of the methods, i.e., buffered HF treatment, is chosen to clean the ablation debris.[12] It needs a long etching time to eliminate the debris once they attach to the surface, which will increase the surface roughness around the mitigated site, and reduce the damage resistance of optics.[12] This method is only suitable for the surface with tiny debris. The other method is the secondary irradiation (or post-treatment) with CO_2 laser,[6] which can effectively reduce the stress and eliminate the debris. It mainly depends on the re-melting process during the second

*Project supported by the National Natural Science Foundation of China (Grant Nos. 61505170, 61505171, and 51535003), the Joint Fund of the National Natural Science Foundation of China, the Chinese Academy of Engineering Physics (Grant No. U1530109), and the China Postdoctoral Science Foundation (Grant No. 2016M592709).

†Corresponding author. E-mail: miaoxinxiang.714@163.com

© 2016 Chinese Physical Society and IOP Publishing Ltd

irradiation. That is, the debris will be re-melted and the residual stress will become weak in the second irradiation process. Based on the current results, the further investigation is developed by choosing the parameters for practical process implementation such as the power, the beam size and the exposition time. It is a good choice once the additional disadvantage factors can be avoided.

In this context, the objective of the work that we detail in this paper focuses on the irradiation effect of the secondary irradiation by combining the experimental measurements with numerical simulations. The temperature and stress behavior and the formation mechanisms in the mitigation process and the secondary treatment are investigated.

2. Experimental detail

First, polished fuse silica (Corning HPFS 7980) samples each with a nominal size of 40 mm×40 mm×3 mm are etched in HF solution to remove the re-deposited layer. At least 10 damage sites each with a lateral size of less than 150 μm and a depth of less than 50 μm are produced on the surface by using a Gaussian-shaped pulse operated at 355 nm, with 6.4-ns pulse length and 0.23 mm^2 ($1/e^2$) beam size. Then the damage sites are repaired using a 10.6-μm CO_2 laser by evaporative method. Second, the mitigation sites are irradiated by CO_2 laser when the sample cools down to the ambient temperature. During the mitigation process, the interval time is 1s between the two powers. Table 1 gives the optimized parameters during the mitigation and secondary treatment process. The laser beam at the surface of the sample has a diameter of 2 mm at $1/e^2$ of initial intensity. Then, it changes into 4 mm at the secondary treatment stage. The detailed descriptions are described in Ref. [8]. The substrate without damage site is also irradiated by a laser with the same parameters to provide a comparison site.

Table 1. Parameters used in damage mitigation and the secondary treatment.

Beam size ($1/e^2$)/mm	Power /W	Irradiation time/s	Irradiation times
2	17	4	1
4	28	2	2

The morphology and the debris are observed by a Nikon optical microscope. The stress distribution is measured by PTC-702 stress meter based on Senarmont compensation method. The profile trace of the irradiated site is measured by a stylus profilometer.

Figure 1 gives the typical optical microscopic images of mitigation sites, secondary treatment site and site obtained directly on substrate. It can be clearly seen that the debris is deposited around the site after the mitigation process (see Fig. 1(a)). It is eliminated after the secondary treatment (see Fig. 1(b). However, the lateral size of the crater has already changed as seen from the profile in Fig. 2. The depth and width of mitigated site are 18.4 mm and 720 μm respectively, while the corresponding sizes increase to 13.5 μm and 1250 μm after the secondary treatment. The differences are $\Delta_{\text{depth}} = 4.9$ μm and $\Delta_{\text{width}} = 530$ μm, respectively. Although this process reduces the depth of the crater, it increases the lateral size. In addition, the raised rim initiated in the mitigation process is eliminated in the secondary treatment process as shown in Fig. 2. It is worthwhile to note Figs. 1(c) and 2 in which both the depth and width of site obtained directly on the substrate are smaller than those of the mitigated site.

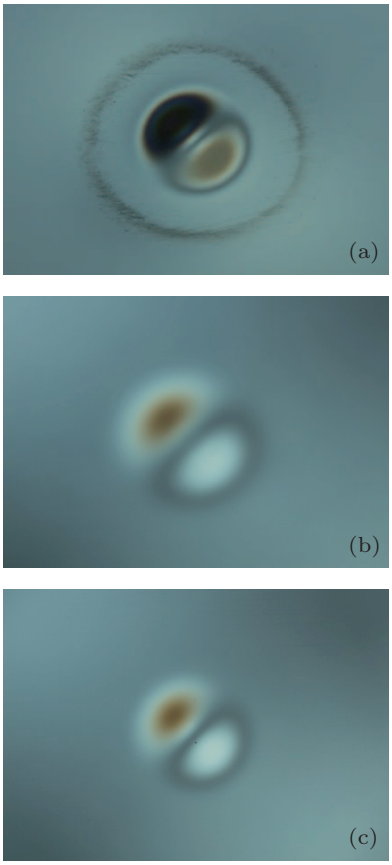


Fig. 1. (color online) Optical microscopic images of mitigation site obtained after damage mitigation (a), secondary treatment (b), and obtained directly on substrate (c).

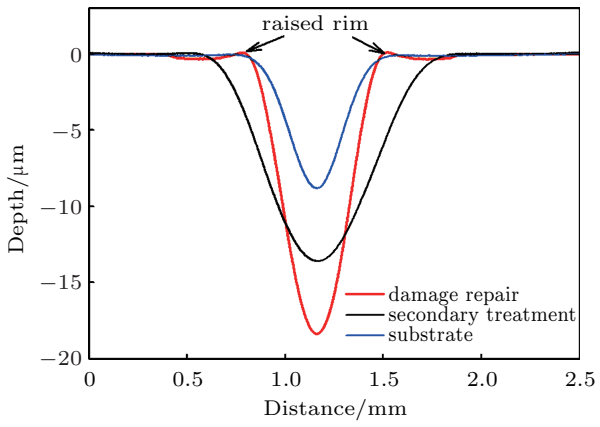


Fig. 2. (color online) Profiles of irradiated site.

Figure 3 presents the residual stress distributions of different states corresponding to Fig. 1. It is clearly seen that the stress affected region is significantly increased after the secondary treatment, while it is smaller than that of the stress obtained directly on the substrate. For the same-size irradiated laser beam and intensity of illumination light source of PTC-702, the more obvious the residual stress, the greater the retardance and residual stress are.[9] However, the stress magnitude lies on the sizes of stress depth and irradiation laser beam in mitigation sites, it is difficult to distinguish the specific difference between the mitigation site and secondary treatment site, which will be quantitatively analyzed by numerical simulation.

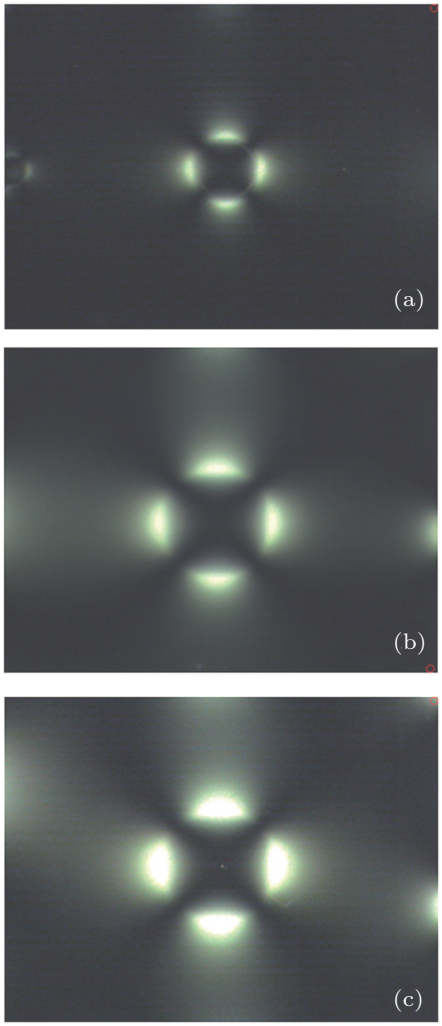


Fig. 3. (color online) Residual stresses of mitigated site obtained after damage repaired (a), secondary treatment (b), and obtained directly on substrate (c).

3. Numerical simulation

3.1. Theoretical foundation

In order to obtain the temperature of amorphous silica due to the deposition of energy by a CO_2 laser, a solution to a couple of partial differential equations is required. The corresponding non-linear heat transfer equation can be expressed as[13]

$$\rho C\frac{\partial T}{\partial t}-K\left[\frac{\partial}{\partial x}\left(\frac{\partial T}{\partial x}\right)+\frac{\partial}{\partial y}\left(\frac{\partial T}{\partial y}\right)+\frac{\partial}{\partial z}\left(\frac{\partial T}{\partial z}\right)\right]=Q, \tag{1}$$

where T, ρ, K, and C are the temperature, density, thermal conductivity and specific heat capacity under constant pressure respectively; Q is the heat source generated during the irradiation of the material. In the case where the Gaussian laser beam depending on position and time irradiates the surface, the Q can be given as follows:

$$Q=\alpha\frac{(1-R)P}{\pi r_0^2}\exp\left(-\frac{x^2+y^2}{r_0^2}\right)\exp(-\alpha z), \tag{2}$$

where r_0 is the radius at which the intensity is $1/e^2$ of the Gaussian beam intensity, P is the incident laser power, R is the Fresnel reflection coefficient depending on the refractive index, and α is the absorption coefficient.

The material displacement is generated during the laser heating of the fused silica due to thermal expansion, which has components in the r and z directions, called μ and w respectively. The correlations of strain-displacement in the case of small displacements are given by[5]

$$\begin{cases}\varepsilon_r=\dfrac{\partial u}{\partial r},\\ \varepsilon_\varphi=\dfrac{u}{r},\\ \varepsilon_z=\dfrac{\partial w}{\partial z},\\ \gamma_{rz}=\dfrac{\partial u}{\partial z}+\dfrac{\partial w}{\partial r},\end{cases} \tag{3}$$

where ε_r, ε_ϕ, and ε_z are the strains in the r, ϕ, z directions and γ_{rz} is the shear strain in the r–z plane. The stress is composed of one shear stress (τ_{rz}) and three normal stresses (σ_r, σ_ψ, σ_z), and it is related to the strain in the case of elastic deformation as follows:

$$\sigma_{ij}=D_{ijkl}\varepsilon_{kl}, \tag{4}$$

where D_{ijkl} is the elasticity tensor, which depends on Young's modulus and Poisson's ratio.

3.2. Physical model

The simulations are conducted by using the commercial software Ansys, which is based on the Finite Element Method. It is a powerful tool in thermo-mechanical coupling simulation. During the simulation, the temperature field is first obtained. Then, the thermal analysis is transformed into structure analysis automatically, and finally, the stress distribution is obtained. The stress distribution acts as an initial condition when the mitigation site is irradiated with the secondary treatment. Thus, the entire simulation includes two processes, that is, damage mitigation and secondary treatment.

To achieve the purpose, a 3D finite model is first built. The entire size is 10 mm×10 mm×1 mm. The heat transfer conduction element solid 90 element with 20 nodes is selected and used to improve the accuracy of the simulation. In addition, the surface convection element surf 152 is selected to serve as a loading element. On the other hand, the non-uniform meshing method is utilized to mesh the model. A finer mesh is placed in the heat-treated zone to ensure the accuracy of the simulation, and a coarser mesh is placed in the remaining part of the structure.

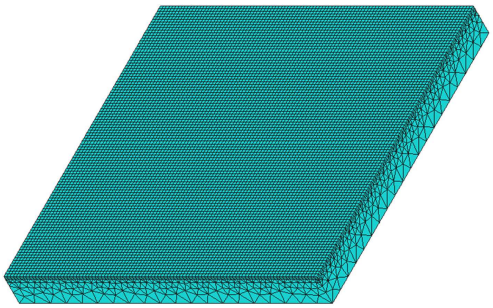


Fig. 4. (color online) Image of physical model and mesh distribution.

3.3. Material property and assumptions

The results strongly depend on the heat conductivity and specific heat capacity, which are temperature dependent. Particularly, the thermal conductivity governs the temperature rise, and it increases with temperature rising, while the density, Young's modulus, Poisson's ratio and expansion coefficient are all constants. The different fused silica parameters used in simulation can refer to Ref. [14].

On the other hand, the model relies on simple but reasonable assumptions. The fused silica material is considered to be isotropic and homogeneous. The phase change and evaporation of material are not taken into account during the irradiation. The evaporated material does not interfere with the incident laser beam. The convection is considered, while the heat transport due to thermal radiation is negligible, and thermal expansion has a negligible effect on heat transfer. The energy is absorbed into the fused silica depth, and the heat is dissipated by conduction. The initial temperature is room temperature (298 K).

3.4. Simulation results

Figure 5 shows the plane and side view image of peak temperature of mitigated site and the secondary treatment site. The temperature distribution of substrate is the same as that of the secondary treatment site given in Fig. 5(b), which is not exhibited here. The temperature evolution of the central irradiation location is given in Fig. 6. To be consistent with the experimental process, the cooling time is taken to be 300 s after the end of irradiation in the simulation process.

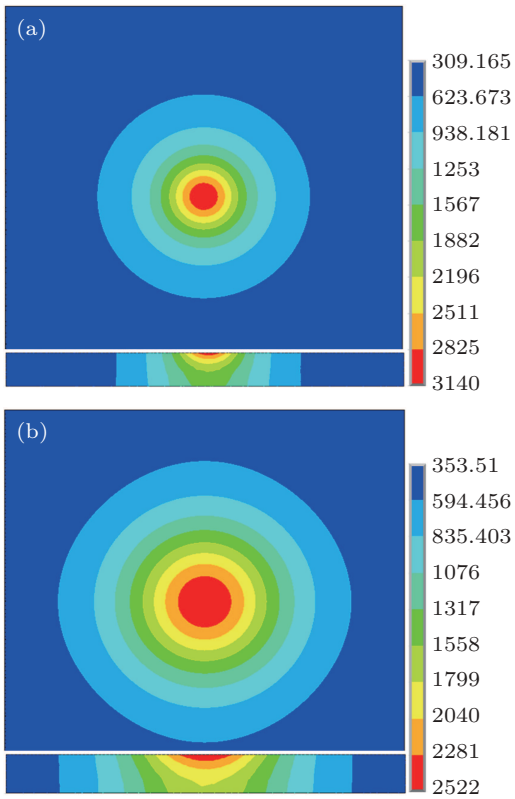


Fig. 5. (color online) Plane and side view image of peak temperature distribution at 4 s in mitigation process (a) and the secondary treatment process at 309 s (b).

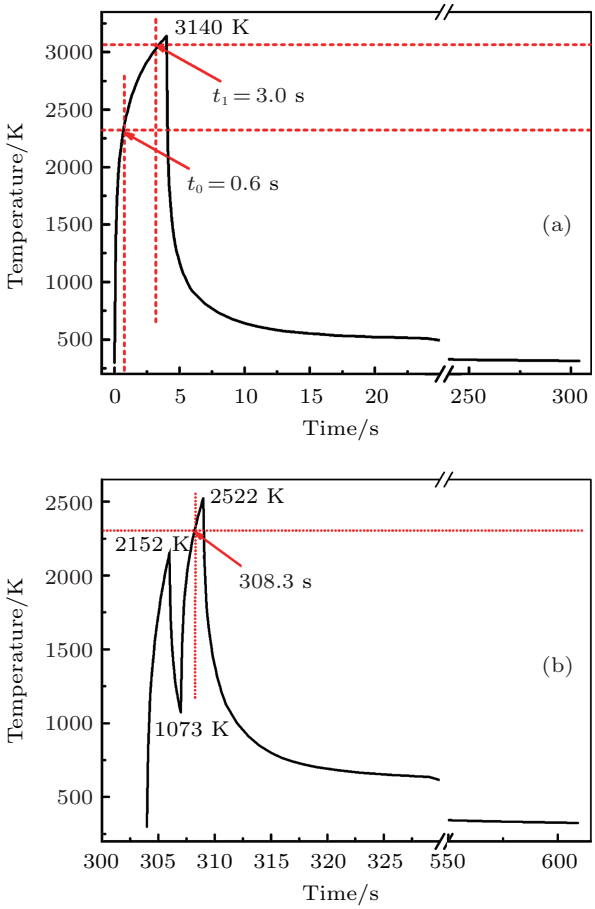


Fig. 6. (color online) Temperature distributions during the damage repair (a) and secondary treatment (b).

It is clearly seen from Fig. 5 that the peak temperature of sample irradiated by 2-mm CO_2 laser is much larger than that by 4-mm CO_2 laser, and their peak temperatures are 3140 K and 2522 K, respectively. However the area of heating region is opposite, a large irradiation laser beam will lead to a larger heating region. As shown in Fig. 6(a), the sample surface temperature arrives at melting point, 2300 K[7] when the sample is irradiated for 0.6 s. The temperature reaches 3140 K for 3 s, which exceeds the evaporative point, 3000 K,[7] the evaporative material will be found around the irradiated region. From Fig. 6(a), it is shown that the total melting time is 2.4 s and the evaporation time is 1 s. The mass movement of material at high temperatures will form the low-viscosity central region outwards, leading to the formation of raised rim, meanwhile the debris will be formed because of the evaporation material re-deposited around the crater at the end of irradiation.[15] The typical ultimate images with debris and their profiles are given in Fig. 1(a) and Fig. 2, respectively.

The temperature distribution of the secondary treatment is given in Fig. 6(b). The peak temperature is 2152 K at the end of the first irradiation. Although it does not reach the melting point, it is much larger than that of soft point (1860 K),[7] and the entire temperature of sample is 1073 K after 1 s cooling time at the end of irradiation as shown in Fig. 6(b). The objective of this irradiation process is mainly to preheat the sample and increase the entire temperature of sample. The reason will be discussed in Section 4. The temperature rises to 2522 K at the end of the second irradiation. The maximum temperature at the irradiation location begins to reach the melting point at 308.3 s. The total effective melting time is 0.7 s in this process as shown in Fig. 6(b).

Figure 7 presents the ultimate steady stress distributions of mitigated site, post-treatment site and the obtained directly on substrate. Figure 8 shows the corresponding stress evolutions with time. Considering the fact that the absolute value of the tensile stress is equal to compressive stress, only the compressive stress is given in Fig. 8. It is shown that the stress has an abrupt transition from compressive stress to tensile stress, which is related to the interaction between stresses in 'solid-like' and 'liquid-like' material regions.[13]

It is clearly seen that the stress distribution and its effected region of mitigated site treated with secondary treatment are larger than those of damage mitigation process, while an even larger stress distribution and affected zone appear on substrate. A comparison between Figs. 3 and 7 shows good agreement between the simulation and experimental results. The calculated stresses are 25.8 Mpa, 9.02 Mpa, and 11.6 Mpa respectively. It is shown that the secondary treatment effectively reduces the residual stress. In addition, although the temperature is the same as those for secondary treatment site and on substrate, the stress obtained on substrate is larger than that of the secondary treatment site. The essential reasons will be discussed in Section 4.

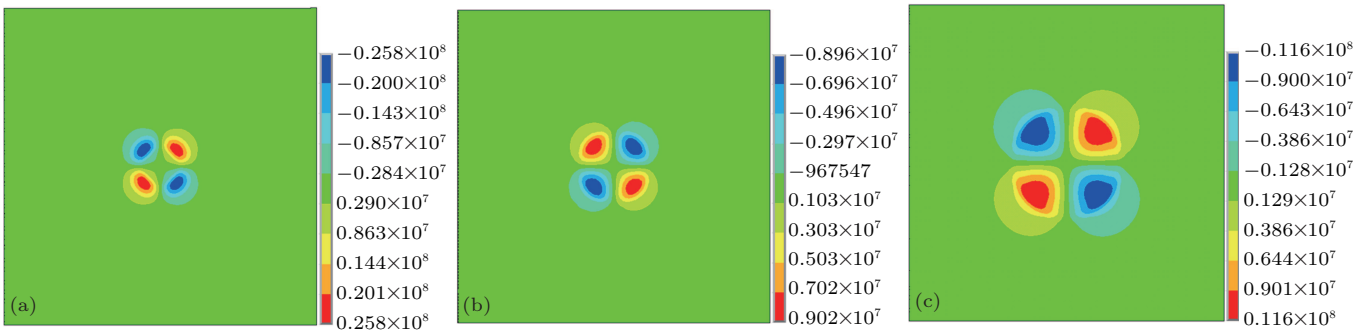


Fig. 7. (color online) Simulated residual stresses of mitigated site obtained after damage mitigation (a), secondary treatment (b), and directly on substrate (c).

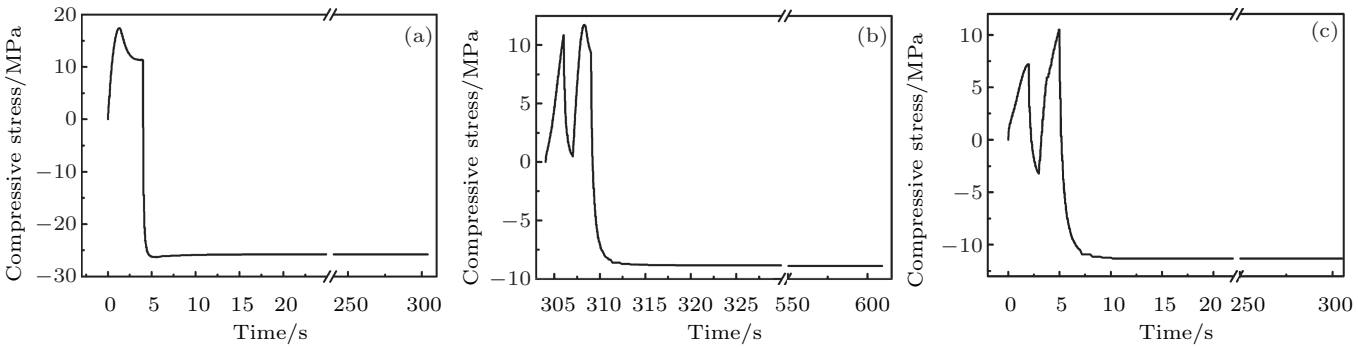


Fig. 8. Residual stress distributions during the damage mitigation (a), secondary treatment (b), and directly on substrate (c).

4. Discussion

The experimental and simulation results indicate that the secondary treatment procedure can not only eliminate the raised rim and reduce the depth of crater, but also eliminate the debris and reduce the residual stress, which mainly depends on the melting process with 0.7 s irradiation at the secondary treatment. As shown in Fig. 6(b), though the material is not melted in the first irradiation process, the material temperature is preheated and increased to 1073 K before the second irradiation. This value is lower than that of the strain temperature (1160 K) of material, moreover, it provides a uniform temperature condition of sample, which can effectively avoid the large strain and stress because of the great gradient of temperature. Meanwhile the melting process during the secondary irradiation can re-melt the debris, raised rim and the material around the crater, the material flow leads to the re-distribution of surface morphology. The operation is also the key procedure to irradiate the site twice with the same laser power.

A stress obtained on substrate is larger than that of mitigation site irradiated with 4-mm CO_2 laser directly as shown in Figs. 3 and 7. It is mainly attributed to the stress that has existed around the mitigation site, the fused silica can be densified as a result of structural relaxation because of local thermal history after the damage mitigation process.[16] The density change can be reversed by secondary treatment. This procedure can completely be regarded as the post-annealing, which can effectively reduce the crater depth and the residual stress.[16] Moreover, it has been proved by Cormont *et al.* that this process can improve the damage threshold of mitigated site.[6] The small stress also reduces the risk of crack propagation when the damage is re-initiated.[9]

Besides the local structural relaxation densification, the mass movement of silica during the secondary treatment is another factor. The radial melting velocity v_r can be expressed as[12]

$$v_r = \frac{\pi^{3/2} r_0^2 T(r)^2 U}{2\eta E^3} P, \tag{5}$$

where r_0 is the radius, $T(r)$ is the surface temperature, U is the latent of evaporation, E is the activation energy, η is the viscosity, and P is pressure. It is shown that the v_r is only related to the radius when the η and P are both constant under constant temperature condition. A large laser beam will lead to a wider mass movement, which results in a large deformation of surface morphology. It can explain why the deformation size obtained by 4-mm CO_2 laser is larger than that by 2-mm CO_2 laser. Considering no loss of material during the secondary treatment, the melting material on the surface will transfer to the bottom of crater, thereby reducing crater depth and eliminating the raised rim, which can reduce downstream modulation. As shown in Fig. 9, the modulation decreases from 16 to 7, and it effectively avoids the appearance of the second peak modulation, which prevents the deleterious intensification on subsequent illumination of downstream optics. The similar results to simulations are reported in Ref. [11].

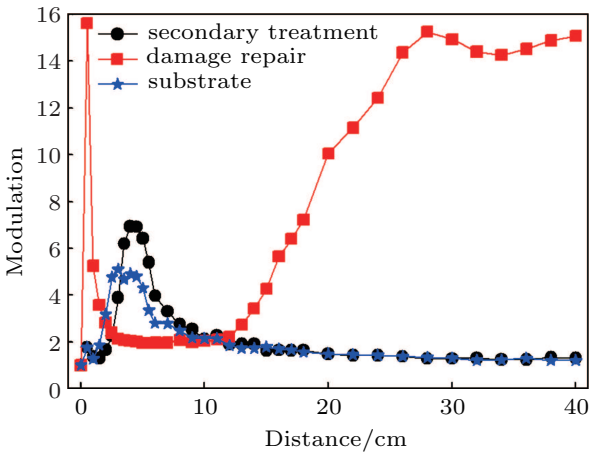


Fig. 9. (color online) Plots of modulation versus distance for different mitigated sites.

For different-size damage sites, the same operation can be used to treat the mitigated site when the debris and raised rim is confined around the site. For example, as shown in Fig. 10, the residual stress is 22.9 Mpa at the end of irradiation with 1-mm CO_2 laser, and then it drops to 7.85 Mpa when it is illuminated by secondary irradiation with 2-mm CO_2 laser. The treatment effect is obvious by this operation.

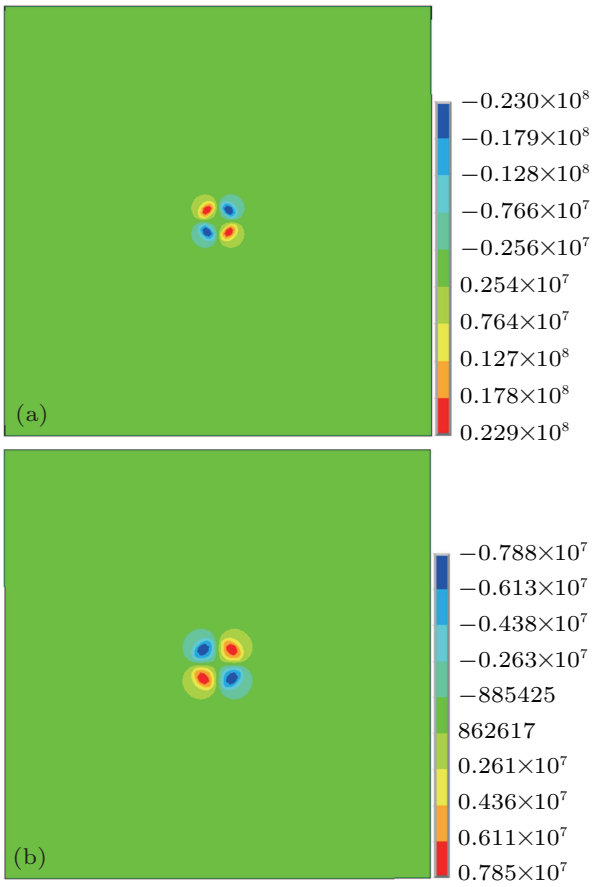


Fig. 10. (color online) Distributions of residual stress during the damage mitigation (a) and secondary treatment (b).

5. Conclusions

The mitigated site is irradiated by secondary treatment with CO_2 laser, it is shown that the experimental results are in agreement with the numerical simulation results. The debris and raised rim around the crater can be effectively eliminated by this method. Moreover, the residual stress can drop 70% of the original stress; it can effectively reduce the probability of crack propagation once the damage of mitigation site is re-initiated. On the other hand, the secondary treatment can increase the lateral size of mitigation site, reduces the crater depth and eliminates the height of the raised rim. Moreover, this process controls the appearance of the large modulation and reduces the damage probability of downstream optics resulting from the modulation.

References

[1] Zhang C C, Zhang L J, Liao W, Yan Z H, Chen J, Jiang Y L, Wang H J, Luan X Y, Ye Y Y and Zheng W G 2015 *Chin. Phys. B* **24** 024220

[2] Sun X Y, Lei Z M, Lu X Q and Fan D Y 2014 *Acta Phys. Sin.* **63** 134201 (in Chinese)

[3] Gao X, Feng G Y, Han J H and Zhai L L 2012 *Opt. Express* **20** 22095

[4] Liu H J, Ye X, Zhou X D, Huang J, Wang F R, Zhou X Y, Wu W D, Jiang X D, Sui Z and Zheng W G 2014 *Opt. Mater.* **36** 855

[5] Gallais L, Cormont P and Rullier J L 2009 *Opt. Express* **17** 23488

[6] Cormont P, Gallais L, Lamaignère L, Rullier J L, Combis P and Hebert D 2010 *Opt. Express* **18** 26068

[7] Mendez E, Nowak K M, Baker H J, Villarreal F J and Hall D R 2006 *Appl. Opt.* **45** 5358

[8] Jiang Y, Xiang X, Liu C M, Luo C S, Wang H J, Yuan X D, He S B, Ren W, Lü H B and Zheng W G 2012 *Chin. Phys. B* **21** 064219

[9] Jiang Y, Xiang X, Liu C M, Wang H J, Liao W, Lv H B, Yuan X D, Qiu R, Yang Y J and Zheng W G 2015 *J. Non-Cryst. Solids* **410** 88

[10] During A, Bouchut P, Coutard J G, Leymarie C and Bercegol H 2006 *Proc. SPIE* **640323** 640323

[11] Bai Y, Zhang L J, Liao W, Zhou H, Zhang C C, Chen J, Ye Y Y, Jiang Y L, Wang H J, Luan X Y, Yuan X D and Zheng W G 2015 *Acta Phys. Sin.* **65** 024205 (in Chinese)

[12] Jiang Y, Xiang X, Liu C M, Yuan X D, Yang L, Yan Z H, Wang H J, Liao W, Lv H B and Zheng W G 2012 *Chin. J. Lasers* **39** 61 (in Chinese)

[13] Vignes R M, Soules T F, Stolken J S, Settgast R R, Elhadj S and Matthews M J 2013 *J. Am. Ceramic Soc.* **96** 137

[14] He S B, Jiang Y, Yuan X D, Wang H J, Liao W, Lv H B, Liu C M, Xiang X, Qiu R and Yang Y J 2014 *Acta Phys. Sin.* **63** 068105 (in chinese)

[15] Dai W, Xiang X, Jiang Y, Wang H J, Li X B, Yuan X D, Zheng W G, Lv H B and Zu X T 2011 *Opt. Lasers Eng.* **49** 273

[16] Feit M D, Matthews M J, Soules T F, Stolken J S, Vignes R M, Yang S T and Cooke J D 2010 *Proc. SPIE* **7842** 78420O